Research Article | Vol. 31, No. 14 / 3 Jul 2023 / Optics Express 22740
Optics EXPRESS

Nonlinear pulse compression of a 200 mJ and 1 kW ultrafast thin-disk amplifier

YANIK PFAFF,[1,2,*] GAIA BARBIERO,[1] MICHAEL RAMPP,[1] SANDRO KLINGEBIEL,[1] JONATHAN BRONS,[3] CATHERINE Y. TEISSET,[1] HAOCHUAN WANG,[1] ROBERT JUNG,[1] JASNA JAKSIC,[1] ABEL H. WOLDEGEORGIS,[1] MAXIMILIAN TRUNK,[4] ANDREAS R. MAIER,[4] CLARA J. SARACENO,[2] AND THOMAS METZGER[1]

[1]*TRUMPF Scientific Lasers GmbH + Co. KG, Feringastr. 10a, 85774 Unterföhring, Germany*
[2]*Photonics and Ultrafast Laser Science, Ruhr University Bochum, Universitätsstr. 150, 44801 Bochum, Germany*
[3]*TRUMPF Laser GmbH, Aichhalder Str. 39, 78713 Schramberg, Germany*
[4]*Deutsches Elektronen-Synchrotron DESY, Notkestr. 85, 22607 Hamburg, Germany*
[*]*yanik.pfaff@trumpf.com*

Abstract: We present a high-energy laser source consisting of an ultrafast thin-disk amplifier followed by a nonlinear compression stage. At a repetition rate of 5 kHz, the drive laser provides a pulse energy of up to 200 mJ with a pulse duration below 500 fs. Nonlinear broadening is implemented inside a Herriott-type multipass cell purged with noble gas, allowing us to operate under different seeding conditions. Firstly, the nonlinear broadening of 64 mJ pulses is demonstrated in an argon-filled cell, showing a compressibility down to 32 fs. Finally, we employ helium as a nonlinear medium to increase the energy up to 200 mJ while maintaining compressibility below 50 fs. Such high-energy pulses with sub-50 fs duration hold great promise as drivers of secondary sources.

1. Introduction

Novel applications such as high harmonic [1] and THz generation [2–4], laser plasma X-ray sources [5], inverse Compton scattering [6] and laser-plasma acceleration of ultra-relativistic electron beams [7–14] demand for increasingly higher pulse energies at pulse durations below 50 fs. In particular, for laser-driven X-ray generation, an increase of the peak intensity by an order of magnitude can account for a 5 to 10-fold higher conversion efficiency [15,16]. Laser-plasma electron acceleration requires a drive laser pulse duration that is resonant to the few-10-fs plasma wavelength and an intensity on the terawatt scale. These stringent experimental requirements were so far predominantly obtained from Ti:Sapphire (Ti:Sa) laser sources, owing to their extremely broad emission bandwidth and thus short pulse durations [11,17,18]. Despite the excellent thermal conductivity of Ti:Sa, such systems remain however limited to moderate average powers [19,20], mostly in the range of 10 to 20 W, and low repetition rates. In particular, their demanding constraints on the pump (high brightness, wavelength in the green) usually impose the use of bulky frequency-doubled solid-state lasers and sophisticated cooling design of the laser crystal, adding to the overall complexity and cost of the system. Most applications would undeniably benefit from higher average power and repetition rates drive laser. Especially, the higher control bandwidth associated with high repetition rate systems would enable feedback loops and active stabilization resulting in improved performance of laser-driven applications [21–23]. In light of this, diode-pumped Yb-doped amplifiers can fulfill these requirements [24,25], albeit with typically longer pulse durations due to the narrowband emission cross section of their gain medium.

#494359 https://doi.org/10.1364/OE.494359
Journal © 2023 Received 27 Apr 2023; revised 31 May 2023; accepted 6 Jun 2023; published 22 Jun 2023

Optics EXPRESS

Among Yb-based systems, thin-disk amplifiers have proven scalability of both pulse energy to above 0.5 J [26–28], and average power to more than 2 kW [29,30]. For such high-energy and high-average-power systems, pulse durations lie between < 500 fs [30] and < 1 ps [26]. Subsequent spectral broadening is therefore necessary to overcome their gain bandwidth limitations and meet the sub-50 fs requirements.

Among others, two approaches have been widely used to extend the spectral bandwidth of high-energy high-average-power Yb-based systems and generate shorter pulse durations: optical parametric amplification (OPA) [31,32] and nonlinear pulse compression induced by the optical Kerr effect and subsequent temporal compression [33]. Due to its limited optical efficiency, the OPA approach is rather unsuitable for achieving high average powers. Commonly used schemes for nonlinear pulse compression at high average powers, instead, rely on waveguides or quasi-waveguides such as fibers, capillaries, or multi-plates [34–40]. The scalability of these waveguides towards high energies and average powers remain a major challenge [41,42]. In recent years, another method for nonlinear pulse compression has become increasingly popular: the Herriott-type multipass cell (MPC) [43–49]. In contrast to other techniques, the MPC-based nonlinear pulse compression combines both scalability to high energies and high optical efficiencies [49–54]. The maximum pulse energy transmitted through a MPC is limited by the fluence on the mirrors and gas ionization and scales linearly with its length [55]. As a result, the MPC allows spectral broadening and, ultimately, also pulse compression of Yb-doped lasers with high average power and high pulse energies at the same time.

Kaumanns *et al.* [51,54] published the highest energy to date, demonstrating spectral broadening and subsequent compressibility in a MPC. Operating near fundamental mode at 5 kHz, they partially compressed 18 mJ pulses from 1.3 ps to 41 fs with an optical efficiency of over 95% [51]. Later, they applied first-order helical Laguerre-Gaussian mode to improve the energy throughput and broaden beyond 100 mJ. The output pulse were compressible from 1.3 ps to 37 fs with an optical efficiency of the multipass setup of >95% [54].

The aim of our work is two-fold: first, push the boundaries of peak power supported by a Yb-based regenerative amplifier and, second, further reduce the pulse duration externally. In this article, we describe in detail our kW-class high-energy Yb-doped ultrafast thin-disk amplifier (Dira 1000-5) and its subsequent nonlinear pulse compression. The Dira 1000-5 laser system delivers at 5 kHz repetition a pulse energy of 200 mJ with sub-500 fs duration. Pulse energies of up to 500 mJ can be extracted from the Dira 1000-5 enabling future experiments with even higher pulse energies.

In this context, we explore the scalability of the nonlinear pulse compression with respect to the pulse energy and average power. The pulses of the Dira 1000-5 undergo nonlinear spectral broadening via self-phase modulation (SPM) in a gas-filled Herriott-type multipass cell. We first experimentally broaden the spectrum of 64 mJ pulses in an argon-filled cell and show its compressibility to 32 fs while maintaining excellent beam parameters. Using helium, we can further increase the pulse energy inside the cell up to 156 mJ and 200 mJ and achieve a corresponding compressibility to 39 fs and 45 fs, respectively. To the best of our knowledge, we present the first nonlinear broadening beyond 150 mJ pulse energy in a Herriott-type multipass cell at a kW-level supporting a near fundamental laser mode.

2. Thin-disk amplifier

The laser source used for the nonlinear pulse compression experiments is a commercial Yb-doped thin-disk regenerative amplifier from TRUMPF Scientific Lasers GmbH & Co. KG [30,56].

A commercial all-fiber-based micro machining laser TruMicro 2000 from TRUMPF Laser GmbH is used for seeding the regenerative chirped pulse amplifier. The seed laser is modified with a customized chirped fiber Bragg grating (CFBG) to stretch the pulses to the nanosecond regime. The subsequent amplifier ring cavity is equipped with two thin-disks continuously

Optics EXPRESS

pumped at 969 nm using low-brilliance industrial diode bars. The switching of the Pockels cell allows to amplify the pulse at each round-trip accounting for high gain. Unfortunately, this is achieved at the expense of the temporal contrast on a nanosecond time scale, creating undesirable satellite pulses. To mitigate this drawback, we implement a pulse picker at the output of the amplifier. Hereby, we can trim the inherent pre- and post-pulses but also enables single-shot and pulse-on-demand operation.

The amplified and chirped output pulses are recompressed by a pair of multilayer dielectric reflection gratings with 1760 lines/mm. The gratings are arranged in a double-pass near Littrow-configuration. The overall optical efficiency of the grating compressor is >90%.

Figure 1(a) shows the compressed output power as a function of pump power when we single out the main pulse. After the pulse-picking stage, we measure a drop of the output power by ~7% which can be attributed to the energy content of the suppressed pre- and post-pulses (Fig. 1(b-c)). If operated at 5 kHz, the system delivers up to 1 kW of compressed power after pulse picking, while higher repetition rates lead to nearly 2 kW [30]. We characterize the pulse-to-pulse energy stability by recording over 50,000 consecutive pulses before the compressor at pulse energy level of 220 mJ. From the collected data, we estimate the fluctuations to be ~0.3% (rms).

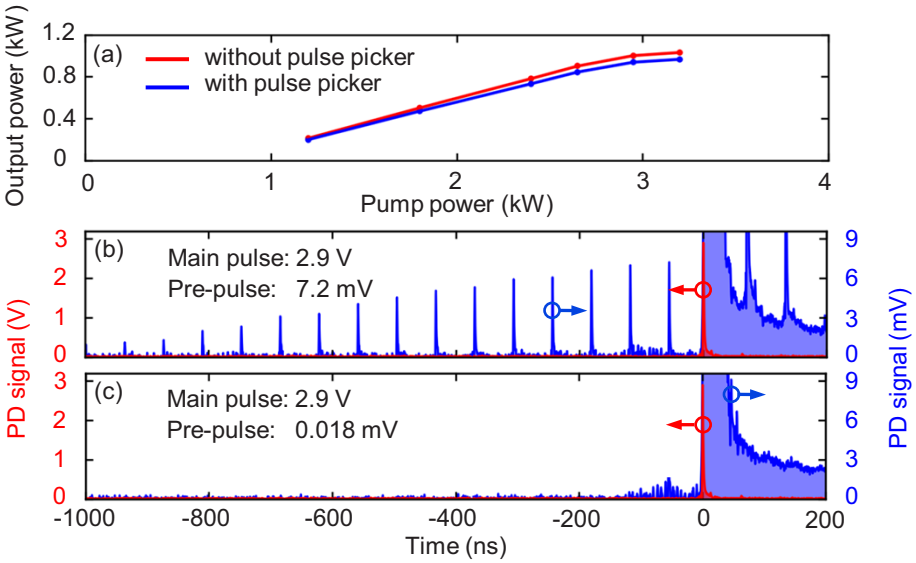

Fig. 1. Characterization of the pre-pulse contrast enhancement. (a) Comparison of power slopes at 5 kHz repetition rate without pulse picker (red) and with pulse picker (blue). The output power was measured after the grating compressor. Full scale photodiode signal (red) and zoomed-in measurement (blue) without pulse picker (b) and with pulse picker (c). The maximum main and pre-pulse intensities without pulse picker (b) and with pulse picker (c) are indicated. The main pulse is centered at 0 ns.

The compressed pulse duration τ_p is retrieved from the measured autocorrelation trace plotted in Fig. 2(b) and is as short as 461 fs. Given the spectral width of the amplified pulses, Fig. 2(a), the pulses are nearly Fourier-transform limited.

We assess the long-term stability of pulse duration by sampling the autocorrelation at 1 Hz, since no device was available to record the shot-to-shot variations, i.e., at a repetition rate of 5 kHz. Within the uncertainty of the commercial autocorrelator, the pulse length fluctuates merely within 2 fs (rms) during the 4-hour log confirming the reliability of our laser source.

Optics EXPRESS

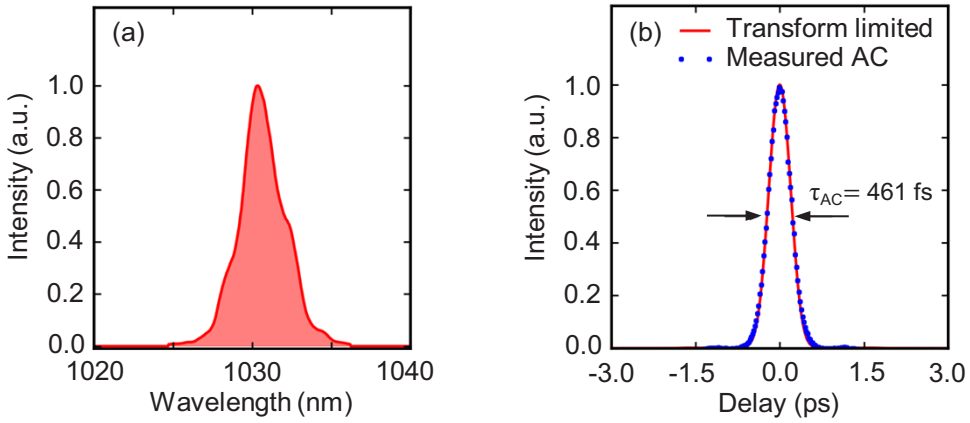

Fig. 2. Spectral and temporal characterization of 200 mJ output pulses. (a) Measured spectrum recorded with a HR4000 spectrometer from Ocean Insight Inc. (b) Autocorrelation (pulseCheck, APE GmbH) trace (blue dotted) and retrieved Fourier-transform limited pulse shape (red).

Preservation of the beam quality despite kW-level average power is confirmed by the computed values of the beam propagation factor being $M^2_{x,y} = 1.42 \times 1.32$ (Fig. 3). Thus, the beam remains nearly diffraction-limited at the output of the compressor.

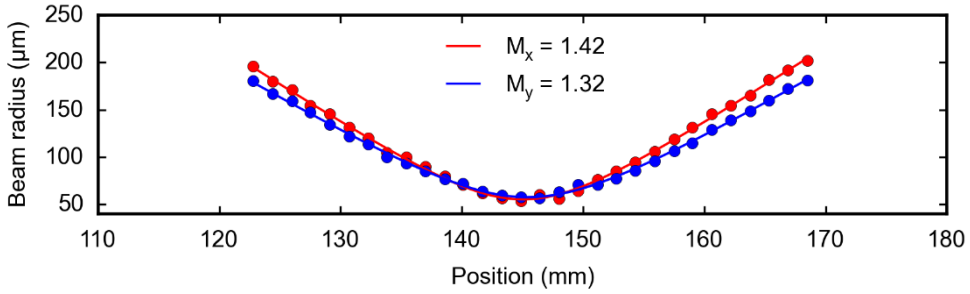

Fig. 3. Measurement of beam propagation factor after the grating compressor at 200 mJ output energy along transverse x (red) and y (blue) axes.

For laser wakefield acceleration, achieving a high temporal contrast is essential [57]. Therefore, we improved the performance of the Dira 1000-5 by diminishing the nanosecond-scale pre- and post-pulses. By adding a pulse picker stage at the output of the regenerative amplifier, we can indeed significantly improve the pre-pulse contrast from the regenerative amplification by over two orders of magnitude, from $\sim 2.5\times10^{-3}$ to $\sim 6.2\times10^{-6}$ as depicted in Fig. 1(b) – (c). This is calculated by comparing the measured photodiode signal (PD) of the main peak with that of the satellite pulses on an oscilloscope. As seen in Fig. 1(c), the fast high voltage switching of the Pockels cell causes a noise signal starting at ~80 ns before the main pulse. Because of the insufficient dynamic range of the oscilloscope, the parasitic pulses cannot be distinguished from the noise floor in Fig. 1(c). We determine the contrast improvement introduced by the pulse picker by suppressing the main pulse and evaluating the resulting attenuation factor. After careful optimization of the Pockels cell alignment and the polarizing optics, the main pulse intensity is lowered by a factor of ~400, which we assume corresponds to the resulting contrast enhancement.

As mentioned in the introduction, we aspire to reach higher pulse intensities and expand the possibilities of future applications. A forthright approach is to boost the output energy of the

Optics EXPRESS

laser source. In the current design of the Dira 1000-5, the maximum pulse energy is limited by the energy storage capacity of the disk. On this account, we simply exchange the two standard disks by thicker ones and apply pulse-pumping at 1 kHz. With these minor modifications, we can amplify the pulses up to 550 mJ [27]. Despite this substantial increase of the Dira 1000-5 output, the resonator design did not require any adjustments and allows for near diffraction-limited beam quality even above 0.5 J. The beam propagation factor remains <1.3 in both axes before entering the grating compressor. These remarkable results attest the exceptional scaling capabilities of the thin-disk concept but also the robustness and thoughtfulness of our design. We underline that the grating compressor in the original product was not meant to support such energies, therefore we were not able to perform the compression at maximum level. Before entering the compressor, we attenuate the output of the amplifier to 1% of the total pulse energy. Figure 4 depicts the final spectrum and the corresponding autocorrelation trace. The output pulse duration is τ_p = 602 fs (Fig. 4(b)), which is close to the Fourier-transform limit (FTL). In a future upgrade, with larger gratings, we expect to provide 600 fs pulses at 0.5 J pulse energy.

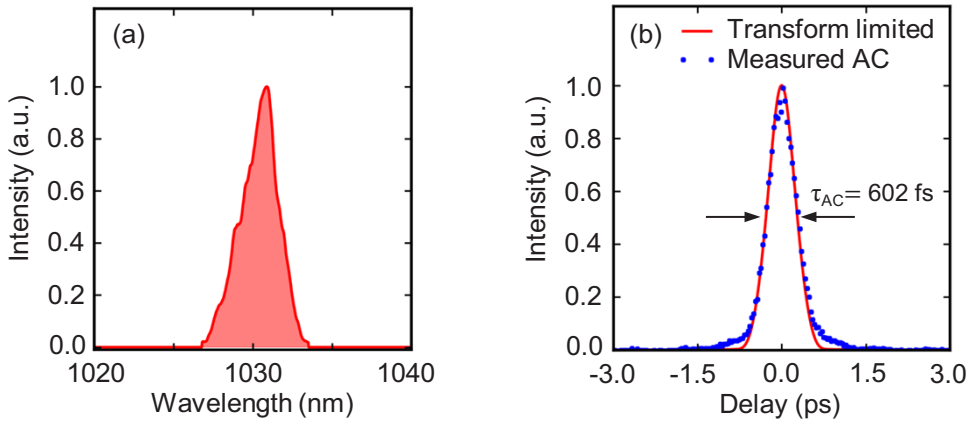

Fig. 4. Spectral and temporal characterization of the pulses amplified to 550 mJ. (a) Measured spectrum, (b) autocorrelation trace (blue dotted) and calculated Fourier-transform limited pulse shape (red) of a compressed 1% sample beam.

3. Multipass cell design

Based on these amplifier performances, we explore the nonlinear compression towards 50 fs at 1 kW average power in a gas-filled Herriott-type multipass cell. Initial spectral broadening simulations were performed to properly scale the MPC for an input energy of 200 mJ and ~500 fs pulse duration which can be delivered by the Dira 1000-5.

Firstly, the MPC was designed to avoid ionization in the focus and secondly to preserve the mirror surface from optical damage at 200 mJ operation. To meet both constraints, a mirror radius of curvature of 5 m and a mirror distance of approximately 10 m were selected. With this arrangement the pulse peak intensity reaches ~200 TW/cm^2 at the focal plane, while the peak fluence approaches 0.5 J/cm^2 on the mirrors surface. Based on the transverse eigenmode inside the MPC, we set the helium pressure to 400 mbar to generate sufficient nonlinear phase shift per pass. Consequently, the on-axis nonlinear phase shift per pass amounts to ~1.8 rad considering a nonlinear refractive index of helium of $n_2 \approx 3.4 \times 10^{-25}$ m^2/W [58].

The spectral broadening was simulated by solving the extended nonlinear Schrödinger equation with a split-step approach as described by Couairon *et al.* [59] including dispersion and Kerr effect. The evolution of the Fourier-transform limited pulse duration of the simulated spectrum over 24 focus passes is shown in Fig. 5. Starting with a FTL of approximately 500 fs, the final

Optics EXPRESS

spectrum supports a pulse duration of ~30 fs after 24 passes. Figure 6(a) shows the initial spectrum and the broadened spectrum after 24 passes. At the MPC output, we estimate an increase of the spectral bandwidth from 8 nm to 106 nm at -20 dB level. Figure 6(b) displays the Fourier-transform limited pulse shapes before and after the MPC. In the simulations performed, the input beam quality was preserved.

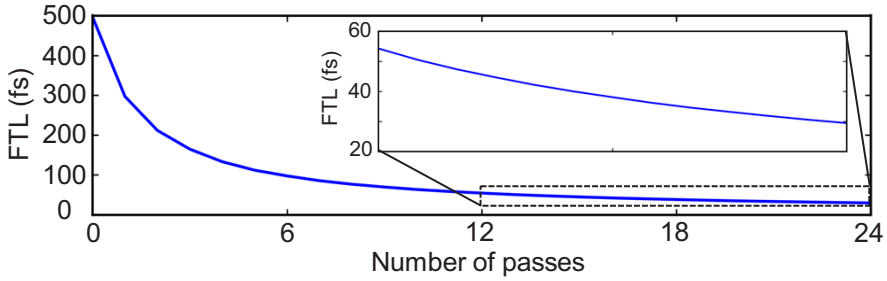

Fig. 5. Evolution of the Fourier-transform limit over the number of focus passes.

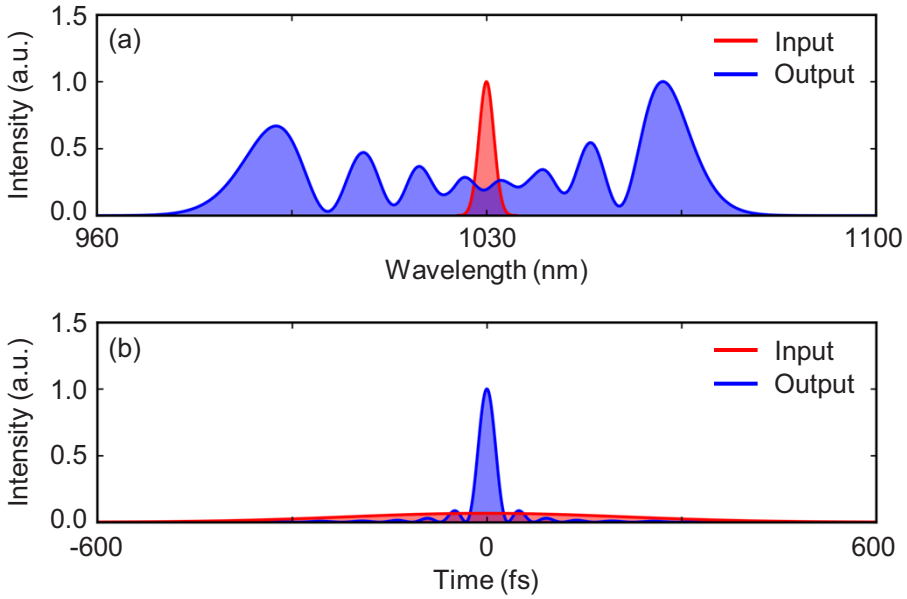

Fig. 6. Simulation results for 200 mJ pulse energy and ~500 fs pulse duration after 24 focus passes. (a) Input (red) and spectrally broadened output (blue) spectrum. (b) Fourier-transform limited pulse shapes of input (red) and output (blue) pulse.

4. Argon-based nonlinear compression

Preliminary spectral broadening experiments in argon allow us to become gradually familiar with the handling and explore the functionality of this MPC aimed originally at 200 mJ operation in helium atmosphere. From our simulations and pre-studies, we expect ionization and optical damage of the mirrors at a lower energy level, at >70 mJ, due to the reduced mode size and optical properties of argon compared to the helium-based arrangement. Hence, the energy coupled into the Herriott-type multipass cell is scaled down to 64 mJ at a repetition rate of 5 kHz, where

Optics EXPRESS

slight ionization occurs. The schematic of the experimental setup is sketched in Fig. 7 for the argon-based nonlinear pulse compression experiments.

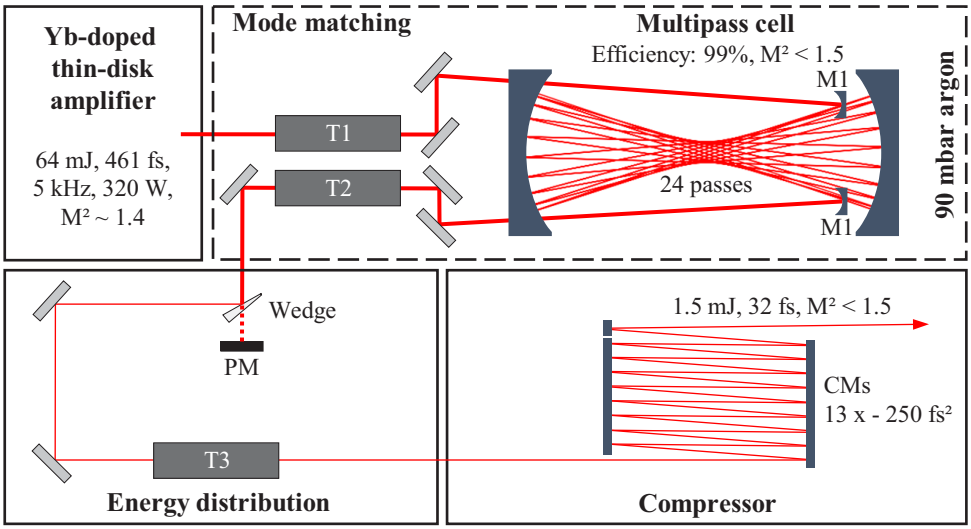

Fig. 7. Schematic layout of the argon-based nonlinear pulse compression setup. The pulses generated by a Yb-doped thin-disk chirped-pulse amplifier are coupled into an argon-filled chamber (dashed line) containing mode matching and recollimation optics and a Herriott-type multipass cell for spectral broadening. Chirped mirrors are used for subsequent temporal recompression at low pulse energy. T1: telescope with 1/3-fold magnification, T2: telescope with 3-fold magnification, T3: telescope with 1/6-fold magnification, M1: in- and outcouple mirrors, PM: power meter, CMs: chirped mirrors.

The mode matching, focusing and recollimation mirrors as well as the multipass cell mirrors are placed in a 12 m long and 0.7 m wide low-pressure chamber. After entering the chamber, a reflective telescope (T1), reduces the beam size by a factor of 3, which is followed by a 10 m ROC concave mirror (M1) to ensure mode-matching with the MPC eigenmode. The MPC consists of 23 identical mirrors with a diameter of 1.5" and a ROC of 5 m, arranged in a circular Herriott-type configuration. The cell features two circular mirror arrangements composed of 12 and 11 mirrors separated by ~9.9 m. In this configuration, the beam diameter ($1/e^2$) is 7.5 mm on the mirror surface and 1.3 mm at the focus position. These mirrors have a reflectivity of >99.99% and a group delay dispersion (GDD) of $|GDD| < 50$ fs^2 between 960 nm and 1100 nm. The chamber was filled with argon at a pressure of 90 mbar. In this work, we assume a nonlinear refractive index for argon of $n_2 \approx 1 \times 10^{-23}$ m^2/W at atmospheric pressure [60] contributing to an on-axis nonlinear phase shift of ~2.6 rad in a single pass and a total B-integral of ~62.4 rad after 24 passes. The beam is guided out of the chamber after recollimation by a second concave mirror and a 3°to°1 magnifying telescope (T2).

The overall outcoupled energy is as high as 63.3 mJ, highlighting the outstanding transmission efficiency property of MPC. Full-energy compression would require a vacuum chamber for the chirped mirror (CM) compressor which was not available at the time of the experiments. To avoid both nonlinear interactions with air and damage on the following chirped mirrors, we perform the pulse compression at ~1.5 mJ after attenuating the beam by an uncoated wedge.

The positive group delay dispersion accumulated through propagation inside the gas-filled MPC and the resulting SPM are compensated by 13 reflections over chirped mirrors introducing a negative GDD of −250 fs^2 per bounce. The low energy compressor accounts for only 1.1% of losses in power. Assuming dispersive mirrors with the same optical specifications were used, we

Optics EXPRESS

can expect an overall optical efficiency of 97.9% for a full-energy compression, including MPC losses.

The compressed pulses are characterized by second-harmonic frequency resolved optical gating (SH-FROG). Figure 8 shows the temporal and spectral characterization of the compressed pulse from the measured spectrograms acquired from a commercial SH-FROG. The retrieval is performed on a 512×512 grid and is associated with an estimated error of 0.47%. The origin of the distinctive peak in the recorded spectrum around the central wavelength at 1030 nm is related to low intensity components in the pulse. Since the contribution of the pre- and post-pulses in this work was reduced by more than two orders of magnitude using a pulse picker, the remaining energy content of the central peak can be attributed to amplified spontaneous emission (ASE) originating from the fiber-based seed source and its subsequent amplification in the regenerative amplifier. A more detailed discussion on the central peak is described in Pfaff *et al.* [53]. The calculated spectral bandwidth at -20 dB stretches over 101 nm. The main pulse contributes to >85% of the energy content based on the retrieved temporal profile, similarly to that of the calculated Fourier-transform limited pulse. The compressed pulse duration is determined to be 31.6 fs, strikingly close its Fourier-transform limit of 30.1 fs. In summary, we are able to

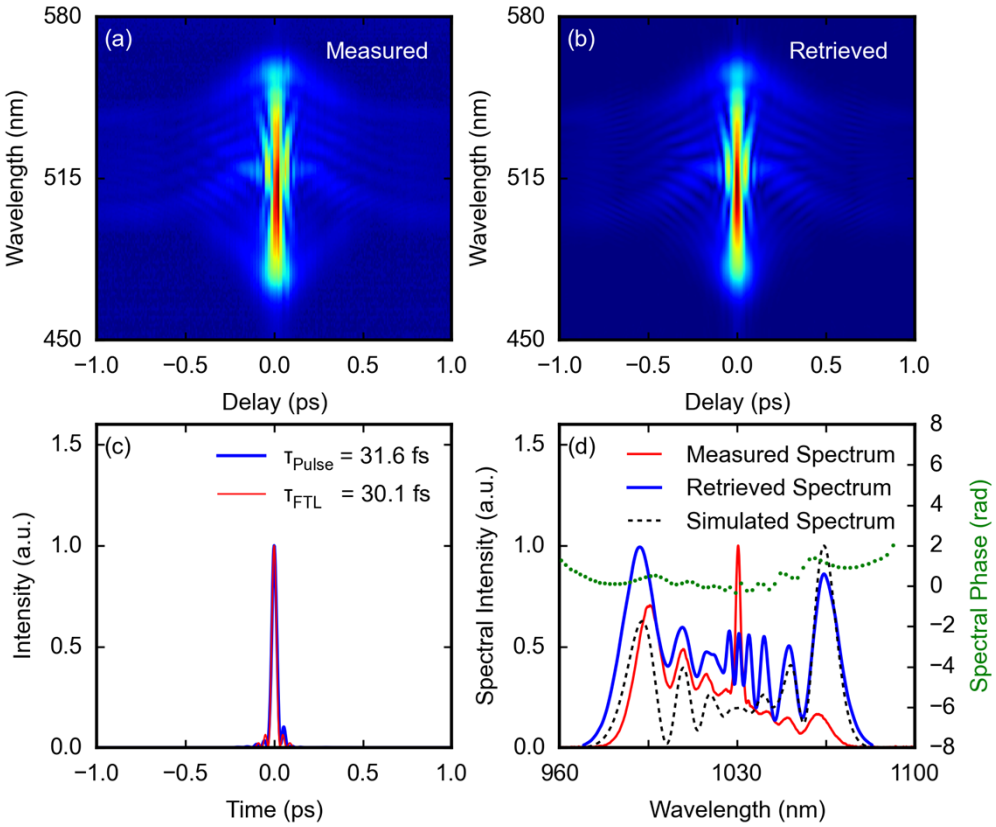

Fig. 8. Temporal characterization of the output pulse from the 64 mJ nonlinear pulse compression setup after the temporal recompression. (a) Measured and (b) retrieved SH-FROG (Mesa Photonics Inc.) spectrogram after the chirped mirror compressor (G-error = 0.47%). (c) Retrieved temporal profile of the compressed pulse. (d) Measured, retrieved, and simulated spectra of the compressed pulses. The green dotted line shows the spectral phase.

Optics EXPRESS

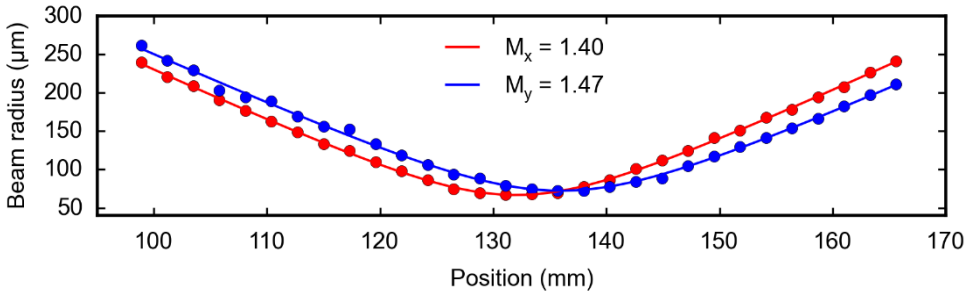

Fig. 9. Measurement of beam propagation factor along transverse x (red) and y (blue) axes after pulse compression of 64 mJ broadened pulses.

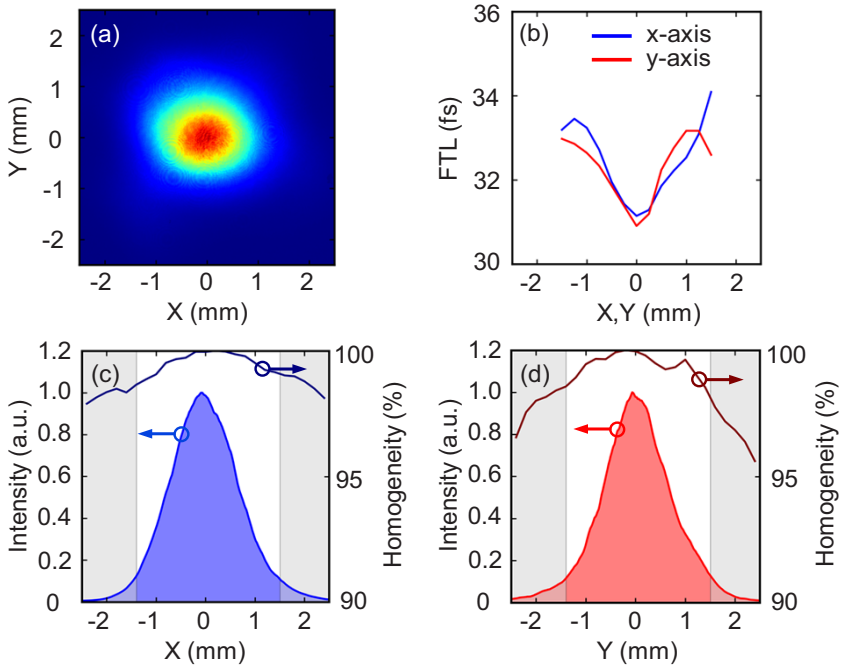

Fig. 10. Spatio-spectral characterization after temporal re-compression of 64 mJ broadened pulses. (a) Transverse beam profile of the collimated and compressed beam. (b) Calculated Fourier-transform limits across two orthogonal axes. The normalized intensity for the x-axis (c) and the y-axis (d) of (a)are represented by the light filled curve. The grey areas mark the positions outside the $1/e^2$ diameter. The dark blue (c) and red (d) curves show the corresponding spatio-spectral homogeneity values.

shorten the pulse length from 461 fs to 31.6 fs, leading to a compression factor of ~15. In case of full-energy compression, the pulse peak power would be increased to 1.6 TW from the 0.11 TW originally provided by 64 mJ input pulses.

The spatial output beam quality is well preserved as proven by the measured M^2 values of the compressed beam, $M^2_{x,y} = 1.40 \times 1.47$ (Fig. 9).

For characterizing the spatio-spectral homogeneity required for a preserving M^2 (Fig. 9), we follow the figure of merit approach described by Weitenberg *et al.* [50], which defines the spectral homogeneity as Homogeneity = $[\int I_\lambda(\lambda) \cdot I_{\lambda 0}(\lambda) d\lambda]^2 / \left[\int I_\lambda(\lambda)^2 d\lambda \cdot \int I_{\lambda 0}(\lambda)^2 d\lambda\right] \times 100$, where each spectrum $I_\lambda(\lambda)$ overlaps with the spectrum on the beam axis $I_{\lambda 0}(\lambda)$. To analyze this

Optics EXPRESS

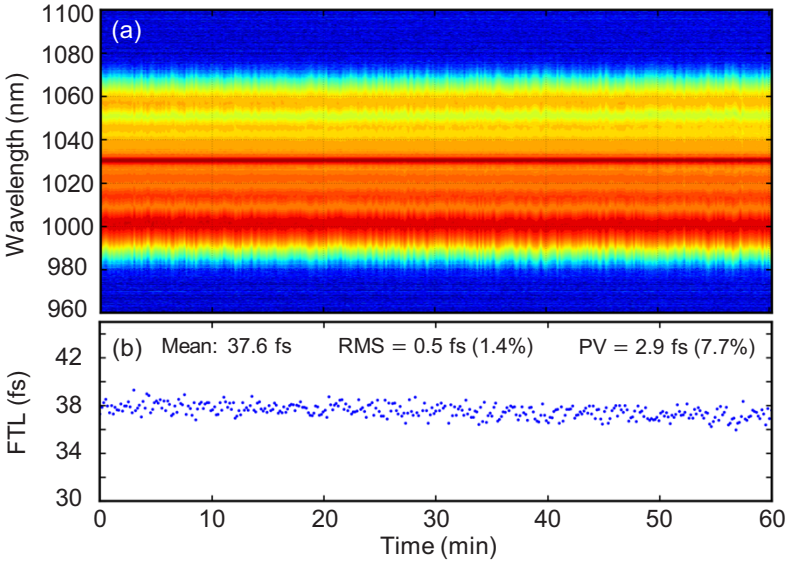

Fig. 11. Characterization of the spectral stability at 50 mJ pulse energy. (a) Spectral performance over 60 min of operation. (b) Fourier-transform limited pulse durations calculated from the spectral data with a mean value of 37.6 fs, a stability of 0.5% (rms) and a peak-to-valley deviation of 7.7%.

spatio-spectral homogeneity, we examined the spectrum in discrete steps across two orthogonal axes of the transverse beam profile. The collimated beam diameters are identical for both axes and equals 2.9 mm (Fig. 10). The spectra are collected, in steps of 0.2 mm, by moving a multimode fiber (200 µm core diameter) mounted behind a 100 µm diameter precision pinhole through the collimated beam. As depicted in Fig. 10(c) – (d), the spatio-spectral homogeneity exceeds 97% in both orthogonal axes within the $1/e^2$ beam diameter, demonstrating the MPC does not alter the input beam quality. The calculated Fourier-transform limits across the two characterized axes of the transverse beam profile are plotted in Fig. 10(b).

Since ionization is already visible at a pulse energy of 64 mJ, we inject only 50 mJ into the MPC to assess the spectral stability. For this measurement, the broadened spectra are logged over 60 min and acquired at a sample rate of 1 Hz with a minimum integration time of 3.8 ms limited by the spectrometer. The system exhibits compelling performance in term of stability as illustrated in Fig. 11. The FTL over one hour of operation is 37.6 fs +/-0.5 fs (rms) and a peak-to-valley deviation of 2.9 fs.

5. Helium-based nonlinear compression

After successfully demonstrating the pulse compressibility up to an input energy of 64 mJ inside an argon-filled MPC, we reconfigure our setup to exploit the full capacities of the Dira 1000-5. Hence, the setup (Fig. 12) was modified in terms of MPC mode size and nonlinear medium compared to the argon-based experiments to avoid optical damage and gas ionization at the maximal pulse energy of 200 mJ at 5 kHz repetition rate.

Similarly, we used two telescopes T1* and T2* with a magnification factor of 1/2.2 and 2.2, respectively. The concave mirrors M1 used to match the eigenmode of the MPC remain unchanged. Finally, the separation between the two circular mirror arrangements is increased to ~9.95 m, leading to a beam diameter of 10 mm at the mirror surface and 1.0 mm at the focus position. At 156 mJ, the chamber is filled with 800 mbar of helium to prevent ionization.

Optics EXPRESS

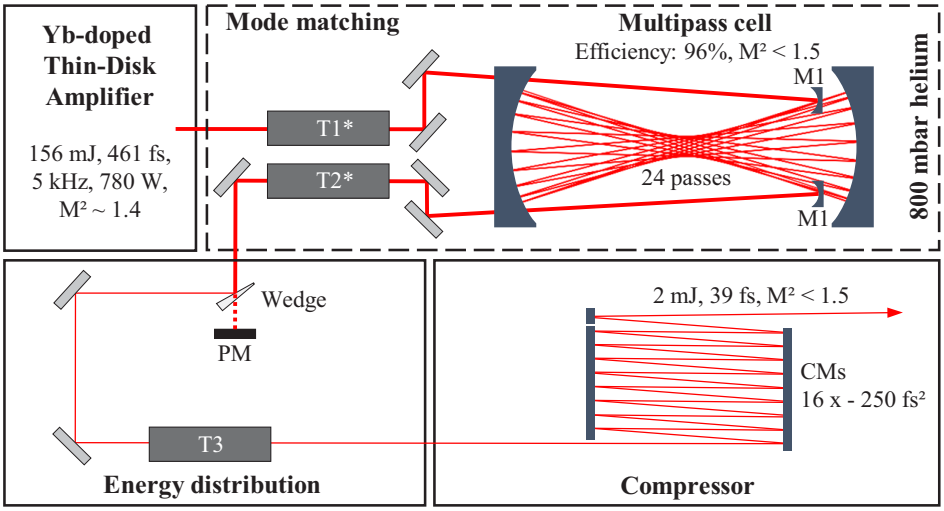

Fig. 12. Schematic layout of the helium-based nonlinear pulse compression setup. The pulses generated by a Yb-doped thin-disk chirped-pulse amplifier are coupled into a helium-filled chamber (dashed line) containing mode matching and recollimation optics and a Herriott-type multipass cell for spectral broadening. Chirped mirrors are used, after the energy attenuation, for subsequent temporal recompression at low pulse energy. T1*: telescope with 1/2.2-fold magnification, T2*: telescope with 2.2-fold magnification, T3: telescope with 1/6-fold magnification, M1: in- and outcouple mirrors, PM: power meter, CMs: chirped mirrors.

With these settings, the on-axis nonlinear phase shift is ~2.1 rad accumulated over a single pass, resulting in a total B-integral of ~50.4 rad after 24 passes. The chamber only introduces minimal losses, so that the transmission still exceeds 96% and the outcoupled pulse energy reaches 150 mJ.

Compression is performed after attenuating the pulses to ~2 mJ and scaling down the beam size by a factor of 6 with a final telescope T3. The compressor consists of the same chirped mirrors as used previously with the argon-filled cell. The total negative GDD is -4000 fs^2 corresponding to 16 reflections. We measured an optical efficiency for the chirped mirror compressor of 98.5%. In combination with the losses of the MPC, an overall optical efficiency of 94.6% could be obtained in case of full-energy compression.

The temporal and spectral characterization of the compressed pulses is shown in Fig. 13. We characterize the pulses using the same 512×512 grid. The retrieval error for this measurement is 0.57%. Seeding with 156 mJ pulses, we demonstrate a compressibility down to 38.8 fs with >85% of the energy included in the main pulse as displayed in Fig. 13. Supposing full-energy compression, the pulse peak power would be increased by a factor of ~12 to 3.3 TW.

We further examine the spatial properties of the compressed beam. The beam quality is well preserved with M^2 values of 1.46 and 1.37 for the x and y-axis, respectively (Fig. 14) indicating a reasonable spatio-spectral homogeneity.

The homogeneity is evaluated according to the same setup described above and is depicted in Fig. 15. Within the $1/e^2$ beam diameter, the homogeneity in both orthogonal axes is determined to be >92%. The Fourier-transform limited pulse duration varies only moderately across the beam.

Finally, we directed the entire output of the Dira 1000-5 into the MPC to test the performance of the cell under such extreme conditions. At 200 mJ, we distinctly witness the onset of ionization via two features. First, we directly observe light scattering in the visible wavelength

Optics EXPRESS

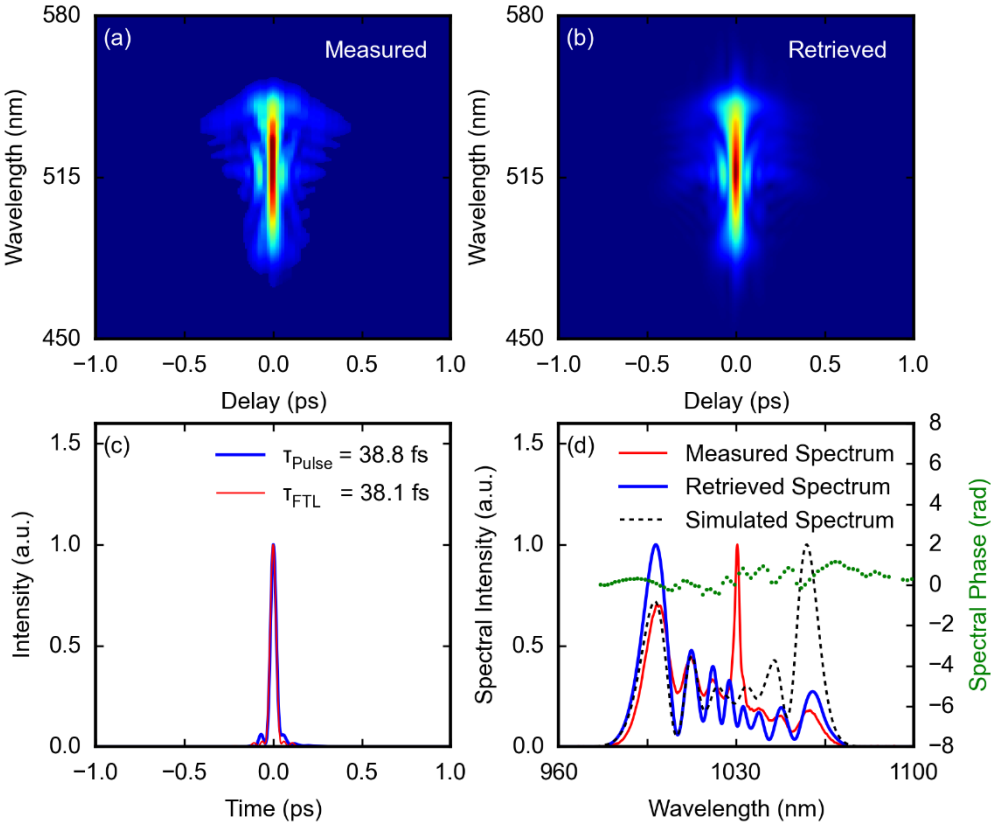

Fig. 13. Temporal characterization of the output pulse from the 156 mJ nonlinear pulse compression setup after the temporal recompression. (a) Measured and (b) retrieved SH-FROG (Mesa Photonics Inc.) spectrogram after the chirped mirror compressor (G-error = 0.57%). (c) Retrieved temporal profile of the compressed pulse. (d) Measured, retrieved, and simulated spectra of the compressed pulses. The green dotted line shows the spectral phase.

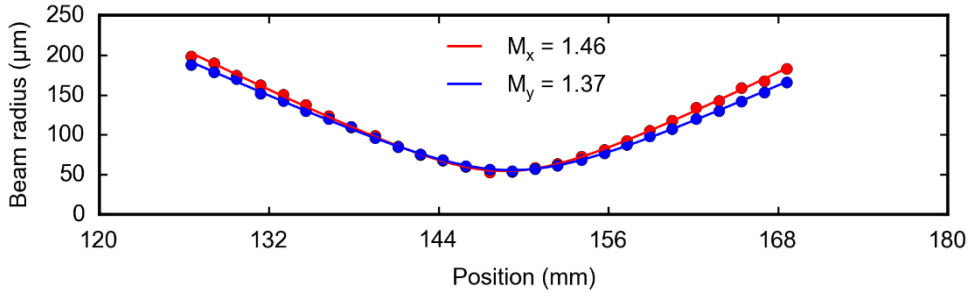

Fig. 14. Measurement of beam propagation factor along transverse x (red) and y (blue) axes after pulse compression of 156 mJ broadened pulses.

Optics EXPRESS

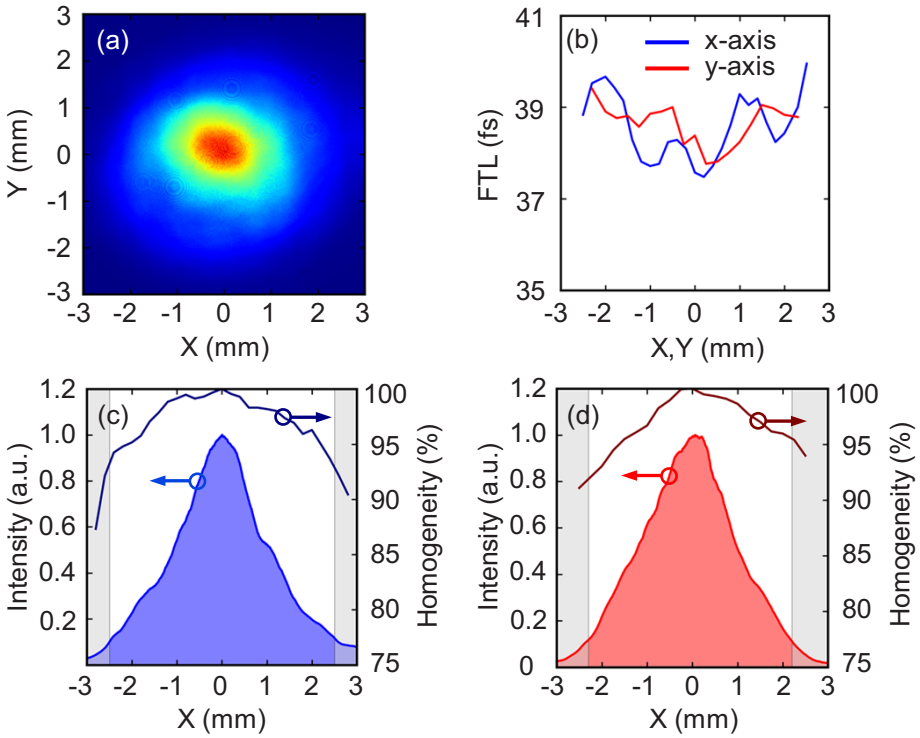

Fig. 15. Spatio-spectral characterization after temporal re-compression of 156 mJ broadened pulses. (a) Transverse beam profile of the collimated and compressed beam. (b) Calculated Fourier-transform limits across two orthogonal axes. The normalized intensity for the x-axis (c) and the y-axis (d) of (a) are represented by the light filled curve. The grey areas mark the positions outside the $1/e^2$ diameter. The dark blue (c) and red (d) curves show the corresponding spatio-spectral homogeneity values.

range within the Rayleigh length along with a slight M^2 degradation (Fig. 16). Second, the temporal characterization (Fig. 17) reveals uncompensated third order dispersion, impeding a clean compression of the spectrally broadened pulse. This behavior is in good agreement with the simulation results of Tavella and Mecseki [61]. Since ionization becomes more intense with time, the onset of ionization can be attributed to leakages, causing ambient air to filter into the chamber. These leakages can originate from multiple sources. Vacuum chambers designed for a pressure of 800 mbar do not seal as tight as those intended for ultra-high vacuum range. Due to the transportation and installation requirements, the chamber consists of several individual segments. These segments were assembled on an uneven laboratory floor, making optimal alignment difficult. And lastly, to ensure high flexibility with respect to adjustment and operability, many flanges were installed. These initial technical limitations will be improved in the future.

Despite the onset of ionization, we were able to recompress the pulses below 45 fs using 14 reflections over the chirped mirrors. The beam propagation factor of the compressed output is slightly degraded to a value of ~1.5 (Fig. 16), which is nevertheless remarkable considering the pulse energy coupled in the MPC.

Optics EXPRESS

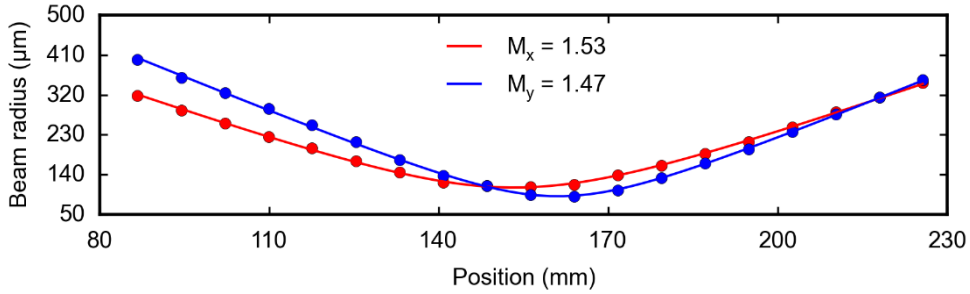

Fig. 16. Measurement of beam propagation factor along transverse x (red) and y (blue) axes after pulse compression of 200 mJ broadened pulses.

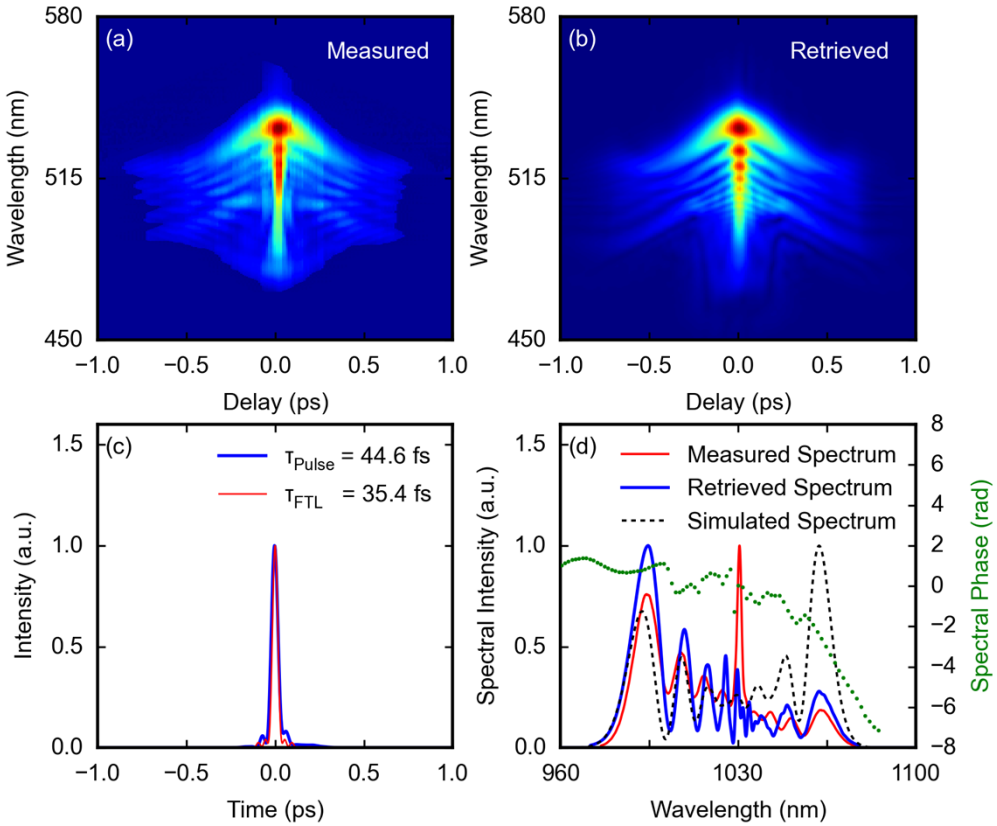

Fig. 17. Temporal characterization of the output pulse from the 200 mJ nonlinear pulse compression setup after the temporal recompression. (a) Measured and (b) retrieved SH-FROG (Mesa Photonics Inc.) spectrogram after the chirped mirror compressor (G-error = 0.93%). (c) Retrieved temporal profile of the compressed pulse. (d) Measured, retrieved, and simulated spectra of the compressed pulses. The green dotted line shows the spectral phase.

Optics EXPRESS

6. Conclusions and outlook

In conclusion, we demonstrate pulse energy scaling and pulse shortening of a commercial Yb-doped thin-disk amplifier. At 5kHz, the original system delivers. a pulse energy of 200 mJ with a pulse duration below 500 fs and a beam quality of M^2 ~1.4. By using an additional pulse picker stage, the pre- and post-pulse contrast on the nanosecond time scale is improved to ~6.2×10^{-6}. Straightforward energy scaling is achieved by simply equipping the amplifier cavity with thicker disks, increasing the pulse energy to 550 mJ. Compression to 602 fs is demonstrated at low energy.

Pulse shortening relies on self-phase modulation in a Herriott-type multipass cell based on nonlinear compression. Using argon, we spectrally broaden the pulses with pulse energies of up to 64 mJ at 5 kHz. The optical efficiency of the MPC is >99%, solely limited by the reflectivity of the mirrors. The initial pulse duration of 461 fs was compressed to 32 fs with an excellent spatio-spectral homogeneity of >97% within the $1/e^2$ diameter. Broadening at higher energy is realized in helium up to 200 mJ and 1 kW of average power. The cell allows a transmission of ~96% of the pulse energy limited by the mirror apertures. Compressibility of the broadened pulses to <45 fs is shown with a preserved beam propagation factor of $M^2 < 1.5$ and a spatio-spectral homogeneity of >90%.

To the best of our knowledge, this is the first experimental demonstration of nonlinear broadening above 150 mJ pulse energy in a Herriott-type multipass cell with nearly diffraction-limited beam quality including a successfully demonstrated compressibility of the pulses to below 39 fs.

In the future, we will review and improve the vacuum chamber design to support nonlinear broadening for even higher energies. In addition, we will build an in-vacuum chirped mirror compressor to perform full-energy compression and implement a high contrast front end to enhance the pulse contrast.

Finally, we aim at reducing the footprint required for the broadening of our joule-class systems [26,28] by investigating novel approaches.

Disclosures. The authors declare no conflicts of interest.

Data availability. Data underlying the results presented in this paper are not publicly available at this time but may be obtained from the authors upon reasonable request.

References

1. M. van Mörbeck-Bock, T. Feng, A. Heilmann, L. Ehrentraut, H. Stiel, M. Hennecke, T. Sidiropoulos, C. von Korff Schmising, S. Eisebitt, and M. Schnürer, "High average power OPCPA MIR-systems for coherent soft x-ray generation accessing absorption edges of metals," Proc. SPIE **11777**, 117770C (2021).
2. F. Meyer, N. Hekmat, T. Vogel, A. Omar, S. Mansourzadeh, F. Fobbe, M. Hoffmann, Y. Wang, and C. J. Saraceno, "Milliwatt-class broadband THz source driven by a 112 W, sub-100 fs thin-disk laser," Opt. Express **27**(21), 30340–30349 (2019).
3. C. Millon, S. Houver, and C. J. Saraceno, "400 kHz repetition rate THz-TDS with 24 mW of average power driven by a compact industrial Yb-laser," Opt. Express **31**(5), 7922–7932 (2023).
4. S. Mansourzadeh, T. Vogel, A. Omar, M. Shalaby, M. Cinchetti, and C. J. Saraceno, "Broadband, high power THz source at 540 kHz using organic crystal BNA," APL Photonics **8**(1), 011301 (2023).
5. R. Keenan, J. Dunn, P. K. Patel, D. F. Price, R. F. Smith, and V. N. Shlyaptsev, "High-repetition-rate grazing-incidence pumped x-ray laser operating at 18.9 nm," Phys. Rev. Lett. **94**(10), 103901 (2005).
6. W. S. Graves, J. Bessuille, P. Brown, S. Carbajo, V. Dolgashev, K.-H. Hong, E. Ihloff, B. Khaykovich, H. Lin, K. Murari, E. A. Nanni, G. Resta, S. Tantawi, L. E. Zapata, F. X. Kärtner, and D. E. Moncton, "Compact x-ray source based on burst-mode inverse Compton scattering at 100 kHz," Phys. Rev. ST Accel. Beams **17**(12), 120701 (2014).
7. A. J. Goers, G. A. Hine, L. Feder, B. Miao, F. Salehi, J. K. Wahlstrand, and H. M. Milchberg, "Multi-MeV Electron Acceleration by Subterawatt Laser Pulses," Phys. Rev. Lett. **115**(19), 194802 (2015).
8. D. Gustas, D. Guénot, A. Vernier, S. Dutt, F. Böhle, R. Lopez-Martens, A. Lifschitz, and J. Faure, "High-charge relativistic electron bunches from a kHz laser-plasma accelerator," Phys. Rev. Accel. Beams **21**(1), 013401 (2018).
9. T. Kurz, T. Heinemann, and M. F. Gilljohann, *et al.*, "Demonstration of a compact plasma accelerator powered by laser-accelerated electron beams," Nat. Commun. **12**(1), 2895 (2021).
10. T. Tajima and J. M. Dawson, "Laser Electron Accelerator," Phys. Rev. Lett. **43**(4), 267–270 (1979).

Optics EXPRESS

11. N. Delbos, C. Werle, I. Dornmair, T. Eichner, L. Hübner, S. Jalas, S. W. Jolly, M. Kirchen, V. Leroux, P. Messner, M. Schnepp, M. Trunk, P. A. Walker, P. Winkler, and A. R. Maier, "Lux – A laser–plasma driven undulator beamline," Nucl. Instrum. Methods Phys. Res., Sect. A **909**, 318–322 (2018).
12. C. G. R. Geddes, C. S. Toth, J. van Tilborg, E. Esarey, C. B. Schroeder, D. Bruhwiler, C. Nieter, J. Cary, and W. P. Leemans, "High-quality electron beams from a laser wakefield accelerator using plasma-channel guiding," Nature **431**(7008), 538–541 (2004).
13. M. G. Ronga, M. Cavallone, A. Patriarca, A. M. Leite, P. Loap, V. Favaudon, G. Créhange, and L. de Marzi, "Back to the Future. Very High-Energy Electrons (VHEEs) and Their Potential Application in Radiation Therapy," Cancers **13**(19), 4942 (2021).
14. F. Albert and A. G. R. Thomas, "Applications of laser wakefield accelerator-based light sources," Plasma Phys. Control. Fusion **58**(10), 103001 (2016).
15. H.-S. Park, D. M. Chambers, and H.-K. Chung, *et al.*, "High-energy Kα radiography using high-intensity, short-pulse lasers," Phys. Plasmas **13**(5), 056309 (2006).
16. Z. Zhang, M. Nishikino, H. Nishimura, T. Kawachi, A. S. Pirozhkov, A. Sagisaka, S. Orimo, K. Ogura, A. Yogo, Y. Okano, S. Ohshima, S. Fujioka, H. Kiriyama, K. Kondo, T. Shimomura, and S. Kanazawa, "Efficient multi-keV x-ray generation from a high-Z target irradiated with a clean ultra-short laser pulse," Opt. Express **19**(5), 4560–4565 (2011).
17. F. Albert, M. E. Couprie, and A. Debus, *et al.*, "2020 roadmap on plasma accelerators," New J. Phys. **23**(3), 031101 (2021).
18. C. M. Heyl, C. L. Arnold, A. Couairon, and A. L'Huillier, "Introduction to macroscopic power scaling principles for high-order harmonic generation," J. Phys. B: At. Mol. Opt. Phys. **50**(1), 013001 (2017).
19. Y. X. Wan, B. T. Fu, H. Q. Xie, S. P. Yu, H. B. Lei, F. B. Zhang, Z. H. Zhang, L. L. Qiao, G. H. Li, J. Zhao, Z. X. Zhao, J. P. Yao, and Y. Cheng, "Observation of rotational coherence in an excited state of CO," Opt. Lett. **46**(16), 3893–3896 (2021).
20. E. Klimešová, O. Kulyk, and Z. Hoque, *et al.*, "A multipurpose end-station for atomic, molecular and optical sciences and coherent diffractive imaging at ELI beamlines," Eur. Phys. J. Spec. Top. **230**(23), 4183–4194 (2021).
21. M. Kirchen, S. Jalas, P. Messner, P. Winkler, T. Eichner, L. Hübner, T. Hülsenbusch, L. Jeppe, T. Parikh, M. Schnepp, and A. R. Maier, "Optimal Beam Loading in a Laser-Plasma Accelerator," Phys. Rev. Lett. **126**(17), 174801 (2021).
22. S. Jalas, M. Kirchen, P. Messner, P. Winkler, L. Hübner, J. Dirkwinkel, M. Schnepp, R. Lehe, and A. R. Maier, "Bayesian Optimization of a Laser-Plasma Accelerator," Phys. Rev. Lett. **126**(10), 104801 (2021).
23. A. R. Maier, N. M. Delbos, T. Eichner, L. Hübner, S. Jalas, L. Jeppe, S. W. Jolly, M. Kirchen, V. Leroux, P. Messner, M. Schnepp, M. Trunk, P. A. Walker, C. Werle, and P. Winkler, "Decoding Sources of Energy Variability in a Laser-Plasma Accelerator," Phys. Rev. X **10**(3), 031039 (2020).
24. S. Nagel, B. Metzger, D. Bauer, J. Dominik, T. Gottwald, V. Kuhn, A. Killi, T. Dekorsy, and S.-S. Schad, "Thin-disk laser system operating above 10 kW at near fundamental mode beam quality," Opt. Lett. **46**(5), 965–968 (2021).
25. H. Stark, J. Buldt, M. Müller, A. Klenke, and J. Limpert, "1 kW, 10 mJ, 120 fs coherently combined fiber CPA laser system," Opt. Lett. **46**(5), 969–972 (2021).
26. C. Herkommer, P. Krötz, R. Jung, S. Klingebiel, C. Wandt, R. Bessing, P. Walch, T. Produit, K. Michel, D. Bauer, R. Kienberger, and T. Metzger, "Ultrafast thin-disk multipass amplifier with 720 mJ operating at kilohertz repetition rate for applications in atmospheric research," Opt. Express **28**(20), 30164–30173 (2020).
27. Y. Pfaff, M. Rampp, C. Herkommer, R. Jung, C. Y. Teisset, S. Klingebiel, and T. Metzger, "Thin-Disk based Regenerative Chirped Pulse Amplifier with 550 mJ Pulse Energy at 1 kHz Repetition Rate," in *Laser Congress 2021 (ASSL, LAC)*, (Optica Publishing Group, 2021), paper AM2A.5.
28. A. Houard, P. Walch, and T. Produit, *et al.*, "Laser-guided lightning," Nat. Photonics **17**(3), 231–235 (2023).
29. J. Dominik, J. Jaksic, K. Ertel, B. Dannecker, M. Scharun, S. Nagel, S. Klingebiel, T. Vogel, C. J. Saraceno, T. Metzger, and D. Bauer, "Thin-disk Multipass Amplifier for 100 mJ Class, Multi-kW High Intensity Lasers," in *Optica High-brightness Sources and Light-driven Interactions Congress* 2022, Technical Digest Series (Optica Publishing Group, 2022), paper HW4B.4.
30. C. Wandt, C. Herkommer, R. Jung, S. Klingebiel, P. Krötz, S. Prinz, M. Rampp, C. Y. Teisset, K. Michel, and T. Metzger, "Ultrafast Thin-Disk based CPA System with >1 kW Output Power and <500 fs Pulse Duration," in *OSA High-brightness Sources and Light-driven Interactions Congress 2020 (EUVXRAY, HILAS, MICS)*, OSA Technical Digest (Optica Publishing Group, 2020), paper HM2B.4.
31. F. Tavella, A. Marcinkevičius, and F. Krausz, "Investigation of the superfluorescence and signal amplification in an ultrabroadband multiterawatt optical parametric chirped pulse amplifier system," New J. Phys. **8**(10), 219 (2006).
32. A. Kessel, V. E. Leshchenko, O. Jahn, M. Krüger, A. Münzer, A. Schwarz, V. Pervak, M. Trubetskov, S. A. Trushin, F. Krausz, Z. Major, and S. Karsch, "Relativistic few-cycle pulses with high contrast from picosecond-pumped OPCPA," Optica **5**(4), 434 (2018).
33. T. Nagy, P. Simon, and L. Veisz, "High-energy few-cycle pulses. Post-compression techniques," Adv. Phys.: X **6**(1), 1307 (2021).
34. R. Safaei, G. Fan, O. Kwon, K. Légaré, P. Lassonde, B. E. Schmidt, H. Ibrahim, and F. Légaré, "High-energy multidimensional solitary states in hollow-core fibres," Nat. Photonics **14**(12), 733–739 (2020).

Optics EXPRESS

35. G. Fan, P. A. Carpeggiani, Z. Tao, G. Coccia, R. Safaei, E. Kaksis, A. Pugzlys, F. Légaré, B. E. Schmidt, and A. Baltuška, "70 mJ nonlinear compression and scaling route for an Yb amplifier using large-core hollow fibers," Opt. Lett. **46**(4), 896–899 (2021).
36. G. Fan, T. Balčiūnas, T. Kanai, T. Flöry, G. Andriukaitis, B. E. Schmidt, F. Légaré, and A. Baltuška, "Hollow-core-waveguide compression of multi-millijoule CEP-stable 32 µm pulses," Optica **3**(12), 1308 (2016).
37. W. Wang, T. Pu, H. Wu, Y. Li, R. Wang, B. Sun, and H. Liang, "High-power Yb:CALGO regenerative amplifier and 30 fs output via multi-plate compression," Opt. Express **30**(12), 22153–22160 (2022).
38. S. Zhang, Z. Fu, B. Zhu, G. Fan, Y. Chen, S. Wang, Y. Liu, A. Baltuska, C. Jin, C. Tian, and Z. Tao, "Solitary beam propagation in periodic layered Kerr media enables high-efficiency pulse compression and mode self-cleaning," Light: Sci. Appl. **10**(1), 53 (2021).
39. G. Barbiero, H. Wang, M. Graßl, S. Gröbmeyer, D. Kimbaras, M. Neuhaus, V. Pervak, T. Nubbemeyer, H. Fattahi, and M. F. Kling, "Efficient nonlinear compression of a thin-disk oscillator to 8.5 fs at 55 W average power," Opt. Lett. **46**(21), 5304–5307 (2021).
40. M. Seidel, G. Arisholm, J. Brons, V. Pervak, and O. Pronin, "All solid-state spectral broadening. An average and peak power scalable method for compression of ultrashort pulses," Opt. Express **24**(9), 9412–9428 (2016).
41. Y.-G. Jeong, R. Piccoli, D. Ferachou, V. Cardin, M. Chini, S. Hädrich, J. Limpert, R. Morandotti, F. Légaré, B. E. Schmidt, and L. Razzari, "Direct compression of 170-fs 50-cycle pulses down to 1.5 cycles with 70% transmission," Sci. Rep. **8**(1), 11794 (2018).
42. C.-M. Chen and P. L. Kelley, "Nonlinear pulse compression in optical fibers. Scaling laws and numerical analysis," J. Opt. Soc. Am. B **19**(9), 1961 (2002).
43. J. Schulte, T. Sartorius, J. Weitenberg, A. Vernaleken, and P. Russbueldt, "Nonlinear pulse compression in a multi-pass cell," Opt. Lett. **41**(19), 4511–4514 (2016).
44. M. Hanna, X. Délen, L. Lavenu, F. Guichard, Y. Zaouter, F. Druon, and P. Georges, "Nonlinear temporal compression in multipass cells. Theory," J. Opt. Soc. Am. B **34**(7), 1340 (2017).
45. A.-L. Viotti, M. Seidel, E. Escoto, S. Rajhans, W. P. Leemans, I. Hartl, and C. M. Heyl, "Multi-pass cells for post-compression of ultrashort laser pulses," Optica **9**(2), 197 (2022).
46. E. Escoto, A.-L. Viotti, S. Alisauskas, H. Tünnermann, I. Hartl, and C. M. Heyl, "Temporal quality of post-compressed pulses at large compression factors," J. Opt. Soc. Am. B **39**(7), 1694 (2022).
47. M. Seidel, P. Balla, C. Li, G. Arisholm, L. Winkelmann, I. Hartl, and C. M. Heyl, "Factor 30 Pulse Compression by Hybrid Multipass Multiplate Spectral Broadening," Ultrafast Science **2022**, 1–10 (2022).
48. M. Müller, J. Buldt, H. Stark, C. Grebing, and J. Limpert, "Multipass cell for high-power few-cycle compression," Opt. Lett. **46**(11), 2678–2681 (2021).
49. C. Grebing, M. Müller, J. Buldt, H. Stark, and J. Limpert, "Kilowatt-average-power compression of millijoule pulses in a gas-filled multi-pass cell," Opt. Lett. **45**(22), 6250–6253 (2020).
50. J. Weitenberg, A. Vernaleken, J. Schulte, A. Ozawa, T. Sartorius, V. Pervak, H.-D. Hoffmann, T. Udem, P. Russbüldt, and T. W. Hänsch, "Multi-pass-cell-based nonlinear pulse compression to 115 fs at 7.5 µJ pulse energy and 300 W average power," Opt. Express **25**(17), 20502–20510 (2017).
51. M. Kaumanns, V. Pervak, D. Kormin, V. Leshchenko, A. Kessel, M. Ueffing, Y. Chen, and T. Nubbemeyer, "Multipass spectral broadening of 18 mJ pulses compressible from 1.3 ps to 41 fs," Opt. Lett. **43**(23), 5877–5880 (2018).
52. A.-L. Viotti, S. Alisauskas, H. Tünnermann, E. Escoto, M. Seidel, K. Dudde, B. Manschwetus, I. Hartl, and C. M. Heyl, "Temporal pulse quality of a Yb:YAG burst-mode laser post-compressed in a multi-pass cell," Opt. Lett. **46**(18), 4686–4689 (2021).
53. Y. Pfaff, C. Forster, G. Barbiero, M. Rampp, S. Klingebiel, J. Brons, C. Y. Teisset, H. Wang, R. Jung, J. Jaksic, A. H. Woldegeorgis, C. J. Saraceno, and T. Metzger, "Nonlinear pulse compression of a thin-disk amplifier and contrast enhancement via nonlinear ellipse rotation," Opt. Express **30**(7), 10981–10990 (2022).
54. M. Kaumanns, D. Kormin, T. Nubbemeyer, V. Pervak, and S. Karsch, "Spectral broadening of 112 mJ, 1.3 ps pulses at 5 kHz in a LG10 multipass cell with compressibility to 37 fs," Opt. Lett. **46**(5), 929–932 (2021).
55. C. M. Heyl, M. Seidel, E. Escoto, A. Schönberg, S. Carlström, G. Arisholm, T. Lang, and I. Hartl, "High-energy bow tie multi-pass cells for nonlinear spectral broadening applications," J. Phys. Photonics **4**(1), 014002 (2022).
56. https://www.trumpf-scientific-lasers.com/.
57. L. Zhang, L.-M. Chen, W.-M. Wang, W.-C. Yan, D.-W. Yuan, J.-Y. Mao, Z.-H. Wang, C. Liu, Z.-W. Shen, A. Faenov, T. Pikuz, D.-Z. Li, Y.-T. Li, Q.-L. Dong, X. Lu, J.-L. Ma, Z.-Y. Wei, Z.-M. Sheng, and J. Zhang, "Electron acceleration via high contrast laser interacting with submicron clusters," Appl. Phys. Lett. **100**(1), 014104 (2012).
58. C. Bree, A. Demircan, and G. Steinmeyer, "Method for Computing the Nonlinear Refractive Index via Keldysh Theory," IEEE J. Quantum Electron. **46**(4), 433–437 (2010).
59. A. Couairon, E. Brambilla, T. Corti, D. Majus, O. d. J. Ramírez-Góngora, and M. Kolesik, "Practitioner's guide to laser pulse propagation models and simulation," Eur. Phys. J. Spec. Top. **199**(1), 5–76 (2011).
60. E. T. J. Nibbering, G. Grillon, M. A. Franco, B. S. Prade, and A. Mysyrowicz, "Determination of the inertial contribution to the nonlinear refractive index of air, N2, and O2 by use of unfocused high-intensity femtosecond laser pulses," J. Opt. Soc. Am. B **14**(3), 650 (1997).
61. F. Tavella and K. Mecseki, "Multi-pass cell spectral broadening at high pulse energies," Phys. Plasmas **29**(8), 083902 (2022).